Hindawi
International Journal of Photoenergy
Volume 2022, Article ID 5288400, 8 pages
https://doi.org/10.1155/2022/5288400

Research Article

Methylammonium Chloride Additive in Lead Iodide Optimizing the Crystallization Process for Efficient Perovskite Solar Cells

Hongqiao Wang[1] **and Jingquan Zhang**[1,2]

[1]*College of Materials Science and Engineering & Institute of New Energy and Low-Carbon Technology, Sichuan University, Chengdu 610065, China*
[2]*Engineering Research Center of Alternative Energy Materials & Devices, Ministry of Education, Chengdu 610065, China*

Correspondence should be addressed to Jingquan Zhang; zhangjq@scu.edu.cn

Received 6 April 2022; Accepted 7 September 2022; Published 29 September 2022

Academic Editor: Jurgen Hupkes

Perovskite solar cells (PSCs) were fabricated using a two-step spin-coating method with MACl added to the inorganic layer. The properties of the perovskite films were characterized by SEM, XRD, PL, UV-vis spectra, etc. The morphology of the PbI_2 film was significantly changed, and the formation of MACl-related intermediate phase was observed at the grain boundaries. The grain size and crystallinity of the perovskite film increased, and the morphology at grain boundaries was optimized, while the composition of perovskite remained unchanged. The introduction of MACl improved the open circuit voltage (V_{OC}) and fill factor (FF) of PSCs, and the optimal device efficiency reached 21.59%. This paper presents a new approach using additives in inorganic layers to optimize the crystallization process for efficient PSCs.

1. Introduction

Since first reported in 2009, PSCs have made great progress with highest photoelectric conversion efficiency (PCE) of 25.7% [1–12]. Additive engineering plays an important role in achieving highly efficient and stable PSCs. MABr coherently incorporates into the lattice of $MAPbI_3$, where Br^- and I^- ions can be combined in any ratio with band gap changing continuously [13, 14], while MACl does not match the lattice of $MAPbI_3$ [15, 16]. As a result, Cl^- ions retain at the surface of perovskite rather than incorporate into the lattice [17–19]. Nevertheless, the introduction of MACl will significantly improve the perovskite film morphology, which may arise from the sublimation of MACl or the loss of intermediate phase formed by MACl at a relatively low temperature [20–23]. Recently, Zuo et al. reported annealing $MAPbI_3$ film in a MACl vapor atmosphere, leading to significantly increased grain size and improved film quality, which confirmed this conjecture from the side [24].

Compared to $MAPbI_3$, $FAPbI_3$ is thermally more stable, with more ideal band gap for high performance PSC. However, phase transition occurs in $FAPbI_3$ below 150°C, where black α-phase becomes photoinactive yellow δ-phase, causing stability issues [8, 25]. Kim et al. reported α-phase $FAPbI_3$ film before annealing by using MACl additive and observed improved film morphology with increased grain size [26].

In the two-step method, two thin film crystallization processes are carried out sequentially, i.e., spin-coating PbI_2 with short time annealing first, then spin-coating FAI with long time annealing, which is different from the one-step method. PbI_2 crystallizes in the first process, and through chemical reaction, perovskite crystallizes in the second [25, 27]. Traditionally, MACl is added to the organic halide precursor (FAI) only [23, 28]. Here, we use MACl as an additive in the inorganic halide precursor (PbI_2). MACl enlarges PbI_2 grains and forms an intermediate phase scattered distributing on the surface of PbI_2. As a result,

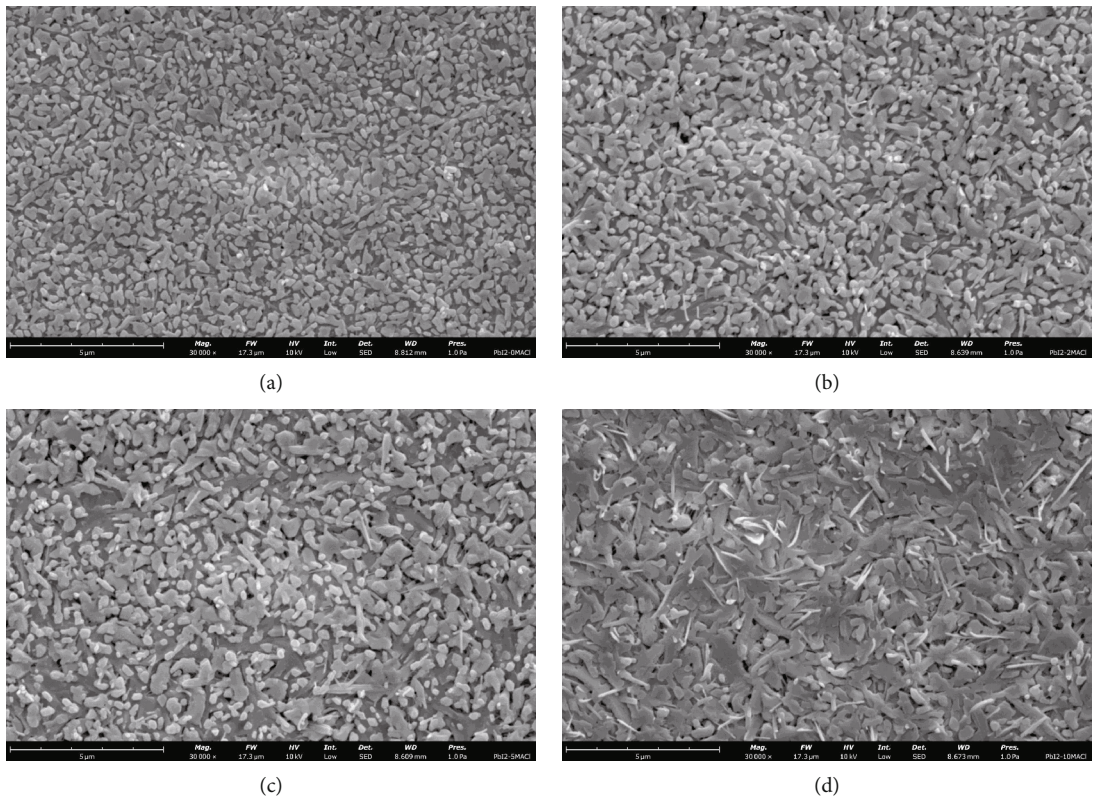

(a) (b) (c) (d)

Figure 1: The surface SEM images of PbI_2 films added different concentrations of MACl: (a) without MACl; (b) with 2 g/L MACl; (c) with 5 g/L MACl; (d) with 10 g/L MACl (scale: 5 μm).

perovskite films are prepared with better morphology, larger grains, higher crystallinity, less defects at grain boundary, longer carrier lifetime, and band gap unchanged. Finally, we fabricate MACl optimized PSC with PCE of 21.59%.

2. Materials and Methods

2.1. Materials. SnO_2 colloidal solution (15 wt% in water) was purchased from Alfa Aesar. N,N-dimethylformamide (DMF), dimethyl sulfoxide (DMSO), isopropanol (IPA), chlorobenzene (CB), acetonitrile (ACN), 4-tert-Butylpyridine (tBP), tris(2-(1H-pyrazol-1-yl)-4-tert-butylpyridine)cobalt(III)tri[-bis(trifluoromethane)sulfonimide] (FK209 Co(III)), and lithium bis(trifluoromethanesulfonyl)imide (Li-TFSI) were purchased from Sigma-Aldrich. PbI_2 (99.99%) was purchased from TCI. Formamidinium iodide (FAI) and methylammonium bromide (MABr) were purchased from GreatCell Solar (Australia). $PbCl_2$, CsI, and methylammonium chloride (MACl) were purchased from Xi'an Polymer Light Technology in China. Spiro-OMeTAD (99.86%) and ITO (7 Ω/sq, $2.5 * 2.5\,cm^2$) were purchased from Youxuan Technology in Liaoning, China.

2.2. Device Fabrication. ITO glass substrates were soaked in deionized water diluted detergent for 3 hours then cleaned by deionized water and ethanol in an ultrasonic cleaner for 30 min, respectively. The ITO glasses were dried by a nitrogen gun and treated with UV-ozone for 15 min before use. 0.5 mL of SnO_2 colloidal solution (15 wt%) was diluted in 1.5 mL of deionized water. SnO_2-based electron transport layer was spin-coated on the precleaned ITO glasses at 4000 rpm for 20 s, followed by annealing at 180°C for 20 min in air. The substrates were then treated with UV-ozone for 12 min before transferring into the glovebox. For the fabrication of perovskite films, a typical two-step sequential deposition method was deployed here. First, 80 μL of PbI_2 precursor solution (600 mg PbI_2, 17.4 mg CsI, and 9 mg $PbCl_2$ dissolved in 0.9 mL of DMF and 0.1 mL of DMSO) was spin-coated on SnO_2 films at 1500 rpm for 30 s. We added 2 mg/5 mg/10 mg MACl to PbI_2 mixture separately before dissolving. The as-prepared FAI/MABr/MACl mixed solution (60 mg FAI, 6 mg MABr, and 6 mg MACl dissolved in 1 mL IPA) was spin-coated on the PbI_2 film at 1700 rpm for 30 s. Afterward, the films were annealed at 150°C for 15 min in a glovebox filled with N_2 gas. After cooling to room temperature, a spiro solution, which consists of 73 mg spiro-OMeTAD dissolved in 1 mL CB, added with 30 μL 4-tert-Butylpyridine, 18 μL Li-TFSI solution (520 mg Li-TSFI in 1 mL of ACN), and 29 μL FK209 Co(III) solution (300 mg FK209 Co(III) in 1 mL of ACN) was deposited on perovskite films at 4000 rpm for 30 s. Finally, 100 nm of Au was thermally evaporated as the electrode under a high vacuum using an electron-beam thermal evaporation system.

2.3. Characterization. The SEM images were obtained by Phenom Pro (Phenom-World B.V.) and the XRD patterns were characterized by DX-2700 (HaoYuana Instrument) using a Cu Kα. The steady-state PL and time-resolved PL

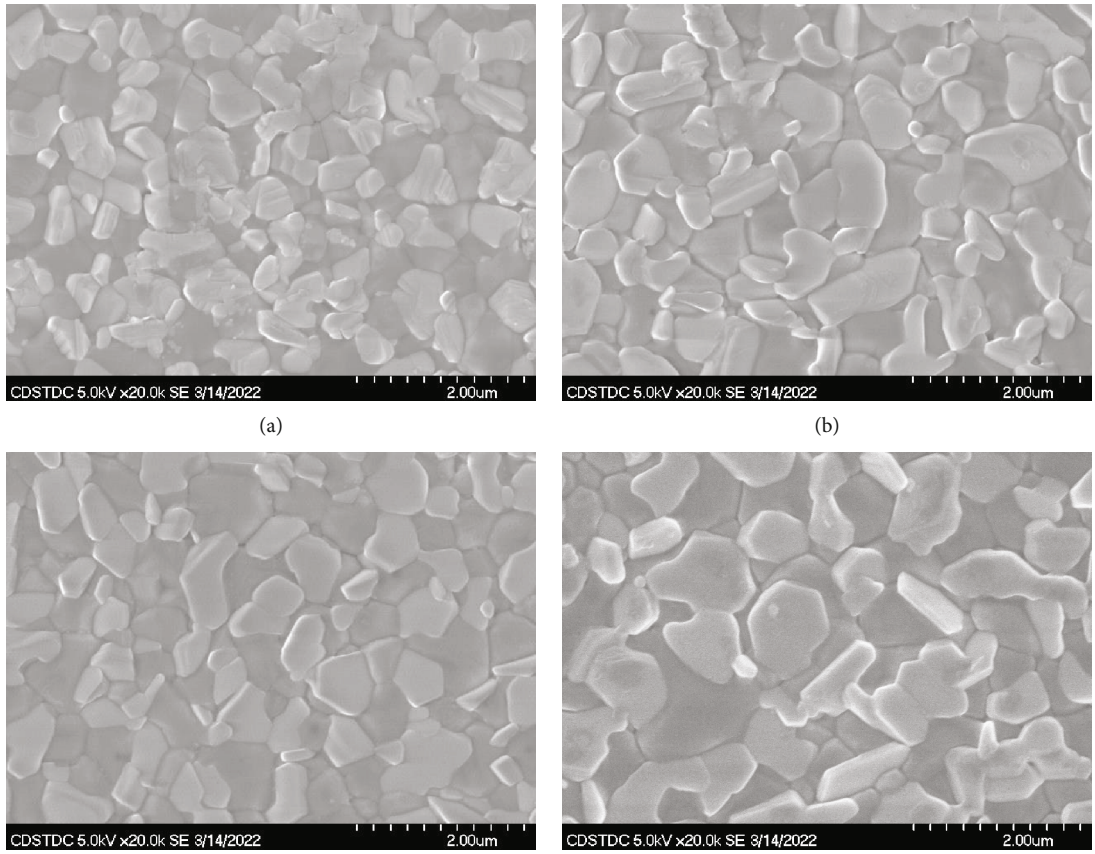

Figure 2: The surface SEM images of perovskite films added different concentrations of MACl: (a) without MACl; (b) with 2 g/L MACl; (c) with 5 g/L MACl; (d) with 10 g/L MACl (scale: 2 μm).

decay were measured by FLS980 (Edinburgh Instruments) with a xenon light at the wavelength of 600 nm and a 655 nm laser excitation source. The J-V curves were characterized under simulated air mass (AM) 1.5G illumination using a solar simulator (Enlitech SS-F5-3A, 100 mW cm^{-2}) and a Keithley 2400 SourceMeter. The solar cells were measured under reverse scan (+1.2 V to −0.1 V) and forward scan (−0.1 V to +1.2 V) with a step of 0.01 V and a delay time of 100 ms.

3. Results and Discussion

3.1. Characterization of Lead Iodide and Perovskite Thin Films. The surface morphology of PbI_2 and perovskite films can be directly observed by the high-resolution SEM. Figure 1 shows the effect of adding different concentrations of MACl on the morphology of the PbI_2 layer: (a) without MACl, (b) 2 g/L MACl, (c) 5 g/L MACl, and (d) 10 g/L MACl. The grains at the bottom of PbI_2 are dense and are loose and small at the surface. After spin-coating the PbI_2 precursor solution, PbI_2 thin film was annealed on a hot plate at 70°C for 13 s. Due to the low annealing temperature, short time and heating from the bottom to the top, PbI_2 grains on the surface were not fully grown. In the cases added with MACl, spindle-shaped grains appeared on the surface of PbI_2 films. With the addition of MACl increasing, size of grains on the surface of PbI_2 increased, and more spindle-shaped grains formed and became thicker. It is especially obvious on the surface of the PbI_2 film added with 10 g/L MACl. The small grains of PbI_2 that were originally granular and dispersed grew into large grains with interconnected and indistinguishable boundaries. Many spindle-shaped grains were attached or embedded in PbI_2 grains.

The composition of the spindle-shaped grains may be MACl or an intermediate phase formed by the reaction of MACl and PbI_2. The intermediate phase is distributed on the surface of the PbI_2 layer and may serve as the nucleation site of perovskite grains during subsequent spin-coating of the organic layer, promoting the formation of the perovskite phase [29–32]. The MACl component in it, sublimed in the subsequent annealing process, may optimize the perovskite film formation process and increase the grain size, which was confirmed in the subsequent experiments.

Figure 2 shows the effect of adding different concentrations of MACl on the surface morphology of the perovskite films prepared by the two-step method: (a) without MACl, (b) 2 g/L MACl, (c) 5 g/L MACl, and (d) 10 g/L MACl. The grain size of the formed perovskite film increases gradually with the increase of the additional amount of MACl. In Figure 2(a), small grains with discontinuous and broken edges exist, and some tiny irregular grains accumulate at the grain boundaries, which can introduce defects. After

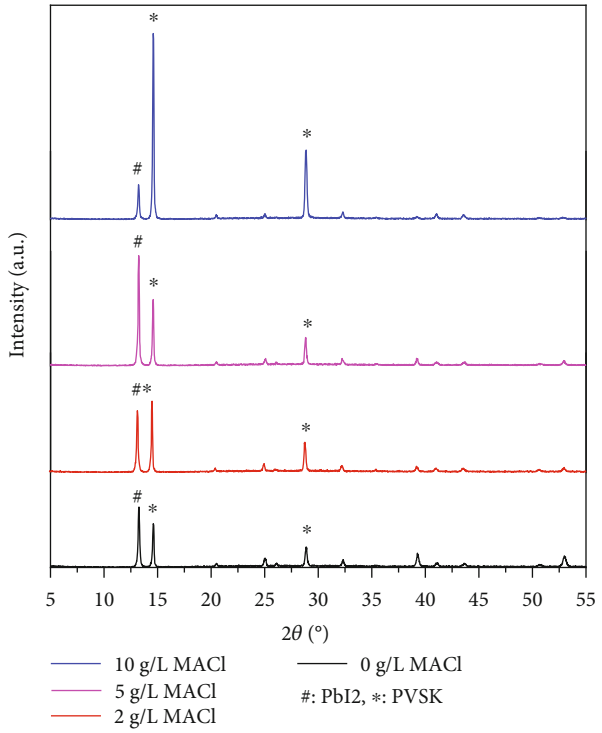

Figure 3: The XRD patterns of perovskite films added different concentrations of MACl.

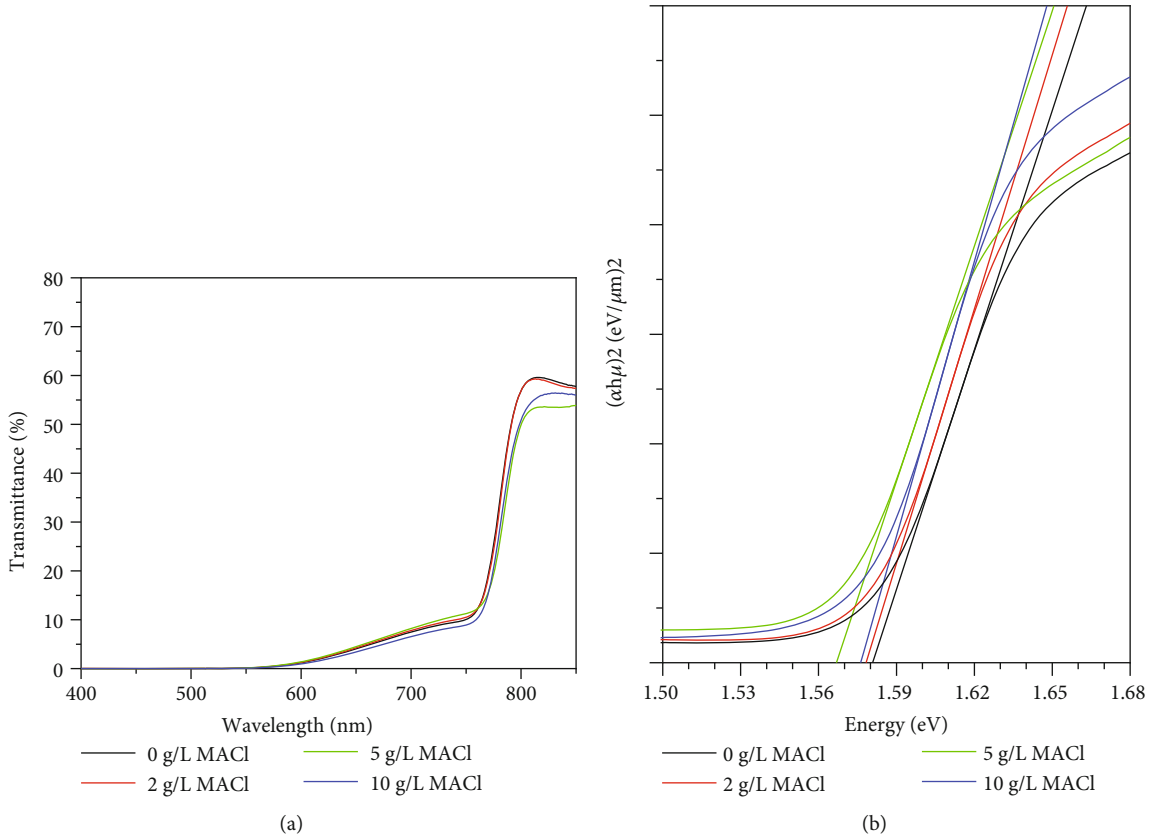

Figure 4: (a) The UV-vis spectra and (b) Tauc curves of perovskite films added different concentrations of MACl.

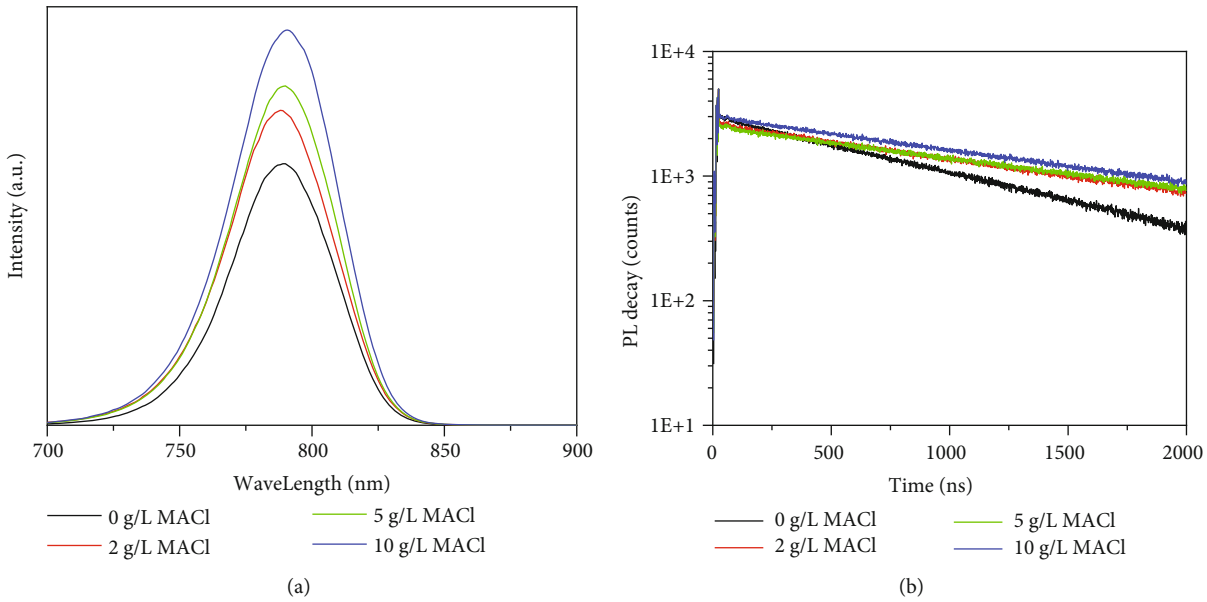

Figure 5: (a) The steady-state PL spectra and (b) TRPL curves of films added different concentrations of MACl (sample structure: corning glass/perovskite).

the addition of MACl, this problem was significantly optimized. On the surface of the perovskite film with 10 g/L MACl added, the grains showed a regular geometric shape, and the grain boundaries were tightly packed. At the same time, large grains mean smaller grain boundary density and therefore less grain boundary defects. The introduction of MACl improves the quality of perovskite thin films by affecting the morphology of the PbI_2 layer and the crystallization process of the perovskite layer, which increases the perovskite grain size and optimizes the morphology at grain boundary.

We performed XRD experiment to test the crystal structure of the perovskite films, as shown in Figure 3. Symbol '#' marks the PbI_2 phase, which corresponds to the (001) crystal plane of PbI_2, and the '*' marks the perovskite phase, corresponding to the (101, 202) planes of the perovskite. The intensity of the diffraction peaks of the perovskite phase increases with the increase of the additional amount of MACl. With 10 g/L MACl addition, the diffraction peak intensity of the perovskite phase is significantly enhanced compared with that of without MACl addition, which indicates that the addition of MACl in the PbI_2 layer promotes the formation of the perovskite phase, which is also consistent with the phenomenon that perovskite grains increase after adding MACl showed in the SEM image, indicating that the crystallinity of perovskite improved. The position of the diffraction peak remains unchanged, so the interplanar spacing remains unchanged according to the Bragg formula $2d\sin\theta = n\lambda$. No diffraction peaks appeared or disappeared, indicating that the crystal structure and phase were remained. The diffraction peak intensity of PbI_2 phase remained basically the same after adding 2 g/L MACl, increased after adding 5 g/L MACl, and decreased but still existed after adding 10 g/L MACl. This is due to the presence of excess PbI_2 in the perovskite film prepared with this precursor ratio, which is beneficial for reducing defects and

Table 1: The double exponential fitting results of TRPL curves of perovskite monolayer films added different concentrations of MACl.

MACl (g/L)	τ_1 (ns)	A_1 (%)	τ_2 (ns)	A_2 (%)	τ_{avg} (ns)
0	131.6	6.1	958.8	93.9	951.5
2	59.56	4.5	1455	95.5	1452.3
5	63.01	5.4	1639	94.6	1635.5
10	87.77	3.3	1586	96.7	1583.2

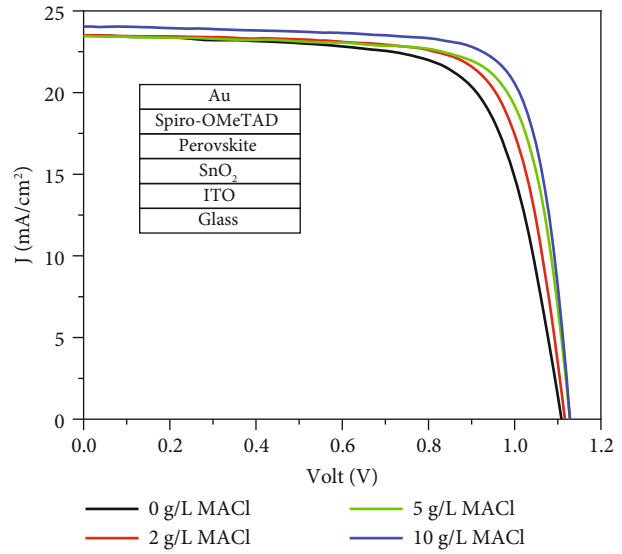

Figure 6: The J-V curves under AM1.5 condition, and the inserted plot shows the device structure of the fabricated perovskite solar cell.

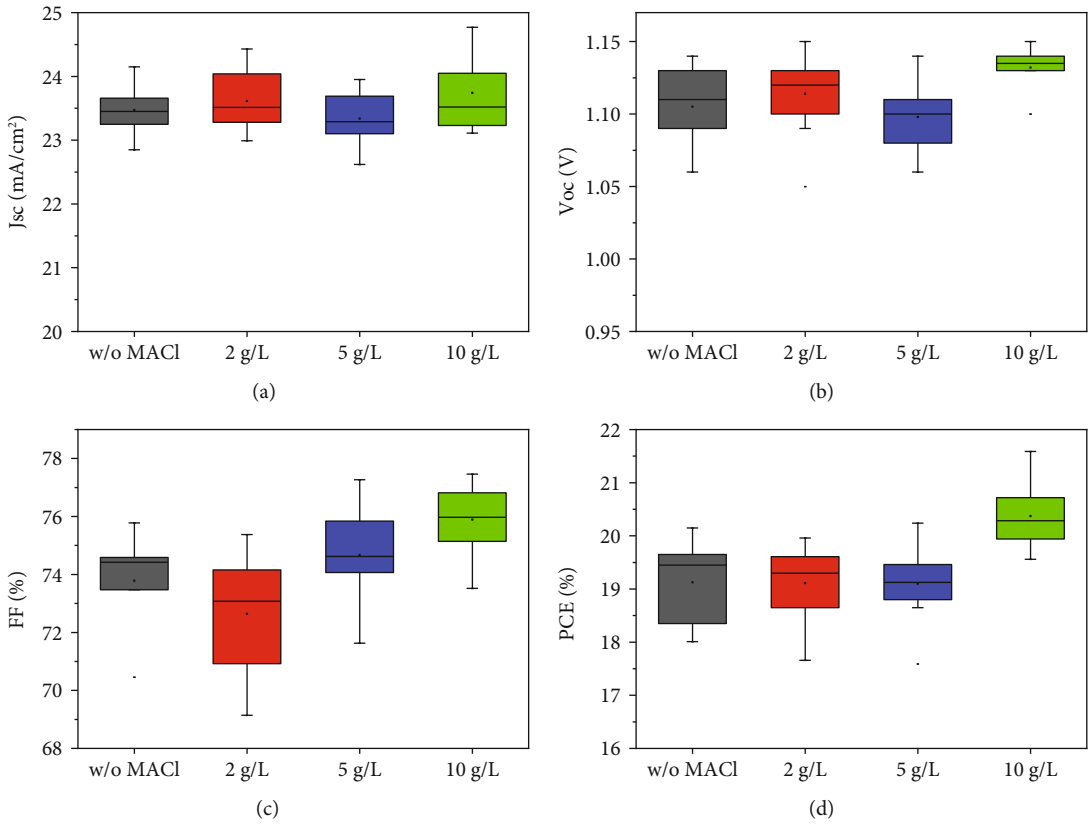

Figure 7: The box charts of photovoltaic parameters of PSCs added different concentrations of MACl: (a) J_{SC}, (b) V_{OC}, (c) FF, and (d) PCE.

improving device performance. On the one hand, it was observed from the SEM that the surface morphology of the PbI_2 layer was changed after the addition of MACl, and there was an intermediate phase formed on the surface of the PbI_2 layer, that is, the influence of MACl mainly affected the surface of the PbI_2 layer, which explained that PbI_2 still exists in the finally formed perovskite film. On the other hand, the intermediate phase on the surface of PbI_2 can act as a nucleation center in the subsequent reaction with the organic layer, and sublimation of MACl can occur during the second step of annealing, which improves the perovskite film formation process and increases the perovskite grain size. Therefore, the diffraction peak intensity of the perovskite phase increases, and the position of the peak does not change.

Figure 4 shows (a) UV-vis transmission spectra and (b) Tauc curves of perovskite films after adding different concentrations of MACl. The transmittance curves of the perovskite films added with different concentrations of MACl basically overlap. According to the Tauc formula, for a direct semiconductor, $(\alpha h\upsilon)^2 = A\,(h\upsilon - \mathrm{Eg})$, where $h\upsilon$ is the incident photon energy, A is a constant, and α is the absorption coefficient. Transmittance $T = I/I_0 = \exp(-\alpha x)$, where I_0 is the intensity of incident light, I is the intensity of out light after absorption by the film, and x is the film thickness. In the Tauc plot in Figure 4, the intercept of the curve on the horizontal axis is the optical band gap Eg of the film. From the Tauc plot, within the error range, the optical band gap of the perovskite films prepared by adding different concentrations of MACl to the PbI_2 layer remains unchanged, indicating that the chlorine atoms do not enter the perovskite lattice, or the amount of entering is very small. This result is similar to the addition of MACl to the organic layer and the addition of MACl to the one-step precursor solution reported in literature, which may be attributed to the lower sublimation temperature of MACl and the large difference in the radii of chloride and iodide ions, which leads to lattice mismatch.

In order to study the effect of MACl on the optoelectronic properties, carrier lifetime, and transport properties of the formed perovskite films, PL and TRPL tests were performed on the perovskite films added with different concentrations of MACl, and the results are shown in Figure 5(a) steady-state PL spectrum and (b) TRPL curve (sample structure: corning glass/perovskite). As the addition of MACl increased, the positions of the PL peaks remained unchanged at 788 nm, corresponding to a band gap of 1.57 eV, which was consistent with the results calculated by the Tauc plot, indicating that the addition of MACl did not change the band gap of the perovskite film. This shows that chlorine atoms do not enter the perovskite lattice or enter in a small amount. The PL intensity gradually increased with the increase of the addition of MACl, indicating that the addition of MACl to PbI_2 may reduce the defect density, thereby weakening the nonradiative recombination, reducing the number of carriers trapped by deep-level defects, and more photoexcited carriers

transition to lower energy levels by radiative recombination and releasing energy in the form of photons. According to the SEM results, as the addition of MACl increases, the grains of the formed perovskite films increase and the grain boundaries become denser, and the irregular grains at the grain boundaries decrease, so the grain boundary density decreases and grain boundary defects decrease, which together lead to the reduction of deep-level defects. That is consistent with the results of PL. TRPL tests were performed on perovskite monolayers with different additions of MACl at a measurement frequency of 0.5 MHz. And we fitted the TRPL curve in Figure 5(b) using the double exponential formula:

$$R(t) = A_1 e^{-(t/\tau_1)} + A_2 e^{-(t/\tau_2)}, \quad (1)$$

where A_1 and A_2 represent the weights of different decay processes and τ_1 and τ_2 correspond to the lifetime of each process. The average lifetime is measured as

$$\tau_{\text{avg}} = \frac{A_1\tau_1^2 + A_2\tau_2^2}{A_1\tau_1 + A_2\tau_2}. \quad (2)$$

The result is showed in Table 1. As the addition of MACl increases, the lifetime of the carriers in the prepared perovskite films gradually increases, indicating that the deep-level defects in the film are reduced and the nonradiative recombination is weakened, which is consistent with the analysis of the PL results. As the addition of MACl further increases, the carrier lifetime tends to be stable, indicating that the perovskite film has been sufficiently passivated.

3.2. Device Fabrication and Performance. The perovskite solar cell devices added with different concentrations of MACl were prepared, and the device structure was ITO/SnO_2/PVSK/Spiro-OMeTAD/Au. The steady-state J-V curves of the device were tested under AM1.5 illumination, as shown in Figure 6. With the increase of MACl addition, the J_{SC}, V_{OC}, and FF of the device all improved, and the best device efficiency of 21.59% was achieved by adding 10 g/L MACl to the PbI_2 layer, corresponding to a fill factor of 77.46%, which benefited from the improved perovskite morphology, increased grain size, and reduced grain boundary defects.

The statistics of device performance with different subcells are shown in Figure 7. The introduction of MACl improves the FF of the cell, and the overall performance of the device with the addition of 10 g/L MACl improves. Due to the improvement of V_{OC} and FF, the PCE of the device is improved. The optimized V_{OC} indicates the density of deep-level defects decreased, and the nonradiative recombination was suppressed.

4. Conclusions

We added different amount of MACl to PbI_2 precursor solution in the two-step spin-coating method. With the addition of MACl, an intermediate phase formed on the surface of PbI_2 and the surface morphology of PbI_2 significantly changed. The intermediate phase can react as nucleation site of perovskite grains or release gaseous MACl during the second annealing process, leading to larger grain size, less grain boundary defect, and better crystallinity, which was confirmed by XRD. Tauc plot and PL both demonstrate that MACl cannot incorporate into the lattice of $FAPbI_3$. With the addition of MACl, carrier lifetime and PL intensity increased, indicating deep-level defect decreased and nonradiative suppressed, which is due to better perovskite film morphology, larger grain size, and less broken in grain boundaries. With the addition of MACl, we fabricated PSC with better performance, especially higher V_{OC} and FF. The PCE of the best device is 21.59%, and the FF is 77.46%.

Data Availability

The data used to support the findings of this study are included within the article. Further data or information is available from the corresponding author upon request.

Conflicts of Interest

The authors declare that there is no conflict of interest regarding the publication of this paper.

Acknowledgments

This work was supported by the Sichuan Provincial Project [grant number: 2021YFG0102]. The authors appreciate the supports from Sichuan University, China, for providing help during the research and preparation of the manuscript.

References

[1] A. Kojima, K. Teshima, Y. Shirai, and T. Miyasaka, "Organometal halide perovskites as visible-light sensitizers for photovoltaic cells," *Journal of the American Chemical Society*, vol. 131, no. 17, pp. 6050-6051, 2009.

[2] J. H. Im, C. R. Lee, J. W. Lee, S. W. Park, and N. G. Park, "6.5% efficient perovskite quantum-dot-sensitized solar cell," *Nanoscale*, vol. 3, no. 10, pp. 4088–4093, 2011.

[3] L. Etgar, P. Gao, Z. Xue et al., "Mesoscopic CH3NH3PbI3/TiO2 heterojunction solar cells," *Journal of the American Chemical Society*, vol. 134, no. 42, pp. 17396–17399, 2012.

[4] M. M. Lee, J. Teuscher, T. Miyasaka, T. N. Murakami, and H. J. Snaith, "Efficient hybrid solar cells based on meso-superstructured organometal halide perovskites," *Science*, vol. 338, no. 6107, pp. 643–647, 2012.

[5] J. H. Heo, S. H. Im, J. H. Noh et al., "Efficient inorganic-organic hybrid heterojunction solar cells containing perovskite compound and polymeric hole conductors," *Nature Photonics*, vol. 7, no. 6, pp. 486–491, 2013.

[6] G. Xing, N. Mathews, S. Sun et al., "Long-range balanced electron- and hole-transport lengths in organic-inorganic CH3NH3PbI3," *Science*, vol. 342, no. 6156, pp. 344–347, 2013.

[7] H. Zhou, Q. Chen, G. Li et al., "Interface engineering of highly efficient perovskite solar cells," *Science*, vol. 345, no. 6196, pp. 542–546, 2014.

[8] J. Jeong, M. Kim, J. Seo et al., "Pseudo-halide anion engineering for α-$FAPbI_3$ perovskite solar cells," *Nature*, vol. 592, no. 7854, pp. 381–385, 2021.

[9] M. Kim, J. Jeong, H. Lu et al., "Conformal quantum dot–SnO2-layers as electron transporters for efficient perovskite solar cells," *Science*, vol. 375, no. 6578, pp. 302–306, 2022.

[10] P.-Y. Gu, N. Wang, C. Wang et al., "Pushing up the efficiency of planar perovskite solar cells to 18.2% with organic small molecules as the electron transport layer," *Journal of Materials Chemistry A*, vol. 5, no. 16, pp. 7339–7344, 2017.

[11] A. A. Said, J. Xie, and Q. Zhang, "Recent Progress in organic electron transport materials in inverted perovskite solar cells," *Small*, vol. 15, no. 27, article e1900854, 2019.

[12] N. Wang, K. Zhao, T. Ding et al., "Improving interfacial charge recombination in planar heterojunction perovskite photovoltaics with small molecule as electron transport layer," *Advanced Energy Materials*, vol. 7, no. 18, article 1700522, 2017.

[13] J. H. Noh, S. H. Im, J. H. Heo, T. N. Mandal, and S. I. Seok, "Chemical management for colorful, efficient, and stable inorganic-organic hybrid nanostructured solar cells," *Nano Letters*, vol. 13, no. 4, pp. 1764–1769, 2013.

[14] N. J. Jeon, J. H. Noh, W. S. Yang et al., "Compositional engineering of perovskite materials for high-performance solar cells," *Nature*, vol. 517, no. 7535, pp. 476–480, 2015.

[15] S. Colella, E. Mosconi, P. Fedeli et al., "MAPbI3-xClxMixed halide perovskite for hybrid solar cells: the role of chloride as dopant on the transport and structural properties," *Chemistry of Materials*, vol. 25, no. 22, pp. 4613–4618, 2013.

[16] H. Yu, F. Wang, F. Xie, W. Li, J. Chen, and N. Zhao, "The role of chlorine in the formation process of "CH3NH3PbI3-xClx" perovskite," *Advanced Functional Materials*, vol. 4, no. 1, pp. 7102–7108, 2014.

[17] H. Min, M. Kim, S. U. Lee et al., "Efficient, stable solar cells by using inherent bandgap of α-phase formamidinium lead iodide," *Science*, vol. 366, no. 6466, pp. 749–753, 2019.

[18] S. M. Yoon, H. Min, J. B. Kim, G. Kim, K. S. Lee, and S. I. Seok, "Surface engineering of ambient-air-processed cesium Lead triiodide layers for efficient solar cells," *Joule*, vol. 5, no. 1, pp. 183–196, 2021.

[19] H. Min, D. Y. Lee, J. Kim et al., "Perovskite solar cells with atomically coherent interlayers on SnO_2 electrodes," *Nature*, vol. 598, no. 7881, pp. 444–450, 2021.

[20] A. Dualeh, P. Gao, S. I. Seok, M. K. Nazeeruddin, and M. Grätzel, "Thermal behavior of methylammonium lead-trihalide perovskite photovoltaic light harvesters," *Chemistry of Materials*, vol. 26, no. 21, pp. 6160–6164, 2014.

[21] S. T. Williams, F. Zuo, C. C. Chueh, C. Y. Liao, P. W. Liang, and A. K. Jen, "Role of chloride in the morphological evolution of organo-lead halide perovskite thin films," *ACS Nano*, vol. 8, no. 10, pp. 10640–10654, 2014.

[22] Y. Zhao and K. Zhu, "CH3NH3Cl-assisted one-step solution growth of CH3NH3PbI3: structure, charge-carrier dynamics, and photovoltaic properties of perovskite solar cells," *Journal of Physical Chemistry C*, vol. 118, no. 18, pp. 9412–9418, 2014.

[23] Q. Chen, H. Zhou, Y. Fang et al., "The optoelectronic role of chlorine in CH3NH3PbI3(cl)-based perovskite solar cells," *Nature Communications*, vol. 6, no. 1, p. 7269, 2015.

[24] W.-W. Zuo, Y.-G. Yang, W.-F. Fu et al., "In situ methylammonium chloride-assisted perovskite crystallization strategy for high-performance solar cells," *ACS Materials Letters*, vol. 4, no. 3, pp. 448–456, 2022.

[25] W. S. Yang, J. H. Noh, N. J. Jeon et al., "High-performance photovoltaic perovskite layers fabricated through intramolecular exchange," *Science*, vol. 348, no. 6240, pp. 1234–1237, 2015.

[26] M. Kim, G.-H. Kim, T. K. Lee et al., "Methylammonium chloride induces intermediate phase stabilization for efficient perovskite solar cells," *Joule*, vol. 3, no. 9, pp. 2179–2192, 2019.

[27] J. Burschka, N. Pellet, S. J. Moon et al., "Sequential deposition as a route to high-performance perovskite-sensitized solar cells," *Nature*, vol. 499, no. 7458, pp. 316–319, 2013.

[28] Q. Jiang, L. Zhang, H. Wang et al., "Enhanced electron extraction using SnO2 for high-efficiency planar-structure HC(NH2)2PbI3-based perovskite solar cells," *Nature Energy*, vol. 2, no. 1, article 16177, 2016.

[29] N. J. Jeon, J. H. Noh, Y. C. Kim, W. S. Yang, S. Ryu, and S. I. Seok, "Solvent engineering for high-performance inorganic-organic hybrid perovskite solar cells," *Nature Materials*, vol. 13, no. 9, pp. 897–903, 2014.

[30] Y. Rong, X. Hou, Y. Hu et al., "Synergy of ammonium chloride and moisture on perovskite crystallization for efficient printable mesoscopic solar cells," *Nature Communications*, vol. 8, no. 1, article 14555, 2017.

[31] M. Abdelsamie, T. Li, F. Babbe et al., "Mechanism of additive-assisted room-temperature processing of metal halide perovskite thin films," *ACS Applied Materials & Interfaces*, vol. 13, no. 11, pp. 13212–13225, 2021.

[32] D. Zheng, T. Zhu, Y. Yan, and T. Pauporté, "Controlling the formation process of methylammonium-free halide perovskite films for a homogeneous incorporation of alkali metal cations beneficial to solar cell performance," *Advanced Energy Materials*, vol. 12, no. 13, article 2103618, 2022.